Available online at www.sciencedirect.com
SCIENCE DIRECT®
Journal of Solid State Chemistry 177 (2004) 3776–3783
JOURNAL OF SOLID STATE CHEMISTRY
www.elsevier.com/locate/jssc

Crystal structure of $Sr_3Ir_2O_7$ investigated by transmission electron microscopy

Hirofumi Matsuhata[a,*], Ichiro Nagai[a,b], Yoshiyuki Yoshida[a,b], Sigeo Hara[a,c], Shin-ichi Ikeda[a], Naoki Shirakawa[a]

[a] *Nanoelectronics Research Institute, Central 2, National Institute of Advanced Industrial Science and Technology, 1-1-1, Umezono, Tsukuba-shi, Ibaraki-ken 305-8568, Japan*
[b] *Japan Society of the Promotion of Science, Chiyoda, Tokyo, 102-8471, Japan*
[c] *College of Science & Technology, Nihon University, 3-25-40, Setagaya, Tokyo, 156-8550, Japan*

Received 17 March 2004; received in revised form 24 June 2004; accepted 25 June 2004
Available online 27 August 2004

Abstract

We report on the crystallographic structure of the layered perovskite iridate $Sr_3Ir_2O_7$, investigated using transmission electron microscopy. The space group was found to be *Bbcb* (D_{2h}^{22}, No. 68 in the International Tables for Crystallography) at 315 K. A very fine twin structure with 90° rotation with respect to the *c*-axis was observed. The crystal structure at temperatures lower than 285 K, where a phase transition from paramagnetism to weak ferromagnetism is known to occur, was also examined. There was no difference in the extinction rule for the diffraction patterns between the two phases. We conclude that there is no change in the space group for this magnetic transition. There still remains the possibility of a change in the rotation angle of IrO_6 octahedrons and a corresponding change in the interatomic distance between Ir and O, though.

Keywords: Bilayered perovskites; Structural distortions; $Sr_3Ir_2O_7$; Electron diffraction; Electron microscopy

1. Introduction

In recent years, the transport and magnetic properties of layered perovskite-type ruthenium oxides have been attracting significant attention since they show interesting behavior. For example, Sr_2RuO_4 shows spin-triplet superconductivity [1,2], and Ca_2RuO_4 is found to be an anti-ferromagnetic Mott-insulator [3]. The layered perovskite type $Sr_3Ru_2O_7$ ruthenium oxides also yield very interesting behavior. On cooling, an increase in the magnetic susceptibility below ~150 K, and a decrease in it at ~20 K are reported [4–9]. This was analyzed as ferromagnetism induced by uniaxial-pressure [10]. While the electrical resistivity is similar to that of metals, it shows a sharp change at ~20 K. This property of $Sr_3Ru_2O_7$ has been discussed as quantum critical behavior [11]. $Ca_3Ru_2O_7$ has been reported to show a phase transition to an anti-ferromagnetic metal at $T_N = 56$ K and to an insulator at $T_M = 48$ K [12]. These properties of the material have been discussed as due to the behavior of the 4*d* electrons of Ru under the influence of a crystal field with the structure distortion.

The physical properties of iridates have also been attracting recent attention, because the similar and related behaviors of 5*d* electrons of Ir are expected. For example, the magnetic properties of $Sr_3Ir_2O_7$ change from paramagnetism to weak ferromagnetism at ~285 K [13–15], and anisotropy in magnetic susceptibility is reported at temperatures lower than 50 K [13]. It is known that perovskite-type compounds are often accompanied by variations in the rotations and tilts of oxygen octahedrons. For example, Sr_2RuO_4 shows no tilt and no rotation of the octahedrons, whereas

*Corresponding author. Fax: +81-29-861-3498.
E-mail address: h.matsuhata@aist.go.jp (H. Matsuhata).

0022-4596/$ - see front matter © 2004 Elsevier Inc. All rights reserved.
doi:10.1016/j.jssc.2004.06.056

$Sr_3Ru_2O_7$ does show a rotation. The rotation changes the interatomic distance between oxygen and the metal atom. The energy levels of the *d*-electrons are related to the crystal lattice structure. Therefore, the determination of the space group and precise structural analysis are important. However, there have been few studies for the refinement of structure analysis for iridates thus far.

The crystal structure of $Sr_3Ir_2O_7$ has been investigated and was found to be Ruddlesden–Popper type with $n = 2$ at first, with $I4/mmm$ for the space group [16,17]. Using X-ray diffraction, Subramanian et al. have reported the possibility of a 12° rotation of the IrO_6 octahedron with respect to the *c*-axis, but they only mentioned $I4/mmm$ as the parent structure, since the expected superlattice reflections were too weak to investigate details. They suggested that the rotations might be a state of disorder [16]. Recently, Cao et al. showed new analysis of the structure using electron diffraction and high-resolution electron microscopy, and indicated the space group to be *Bbca* [13], but details of their analysis were not described in their report. The results by Subramanian et al. may be incomplete for current situation of research work on transport and magnetic properties of this crystal, but results by Cao et al. are inconsistent with that by Subramanian et al., and therefore structure of this crystal remains still to be refined. In this paper, we report on the structure analysis of $Sr_3Ir_2O_7$ using transmission electron microscopy (TEM). Possibility of a crystal lattice change accompanying the observed magnetic transition at ~285 K is also examined.

Fig. 1 shows a unit-cell of the Ruddlesden–Popper type structure with $n = 2$. Spheres represent Sr atoms and octahedrons represent IrO_6. Oxygen atoms are at the corners and Ir atoms are at the centers of the octahedrons. Rotation of the octahedrons is not considered in this structure. Fig. 2(a) represents the

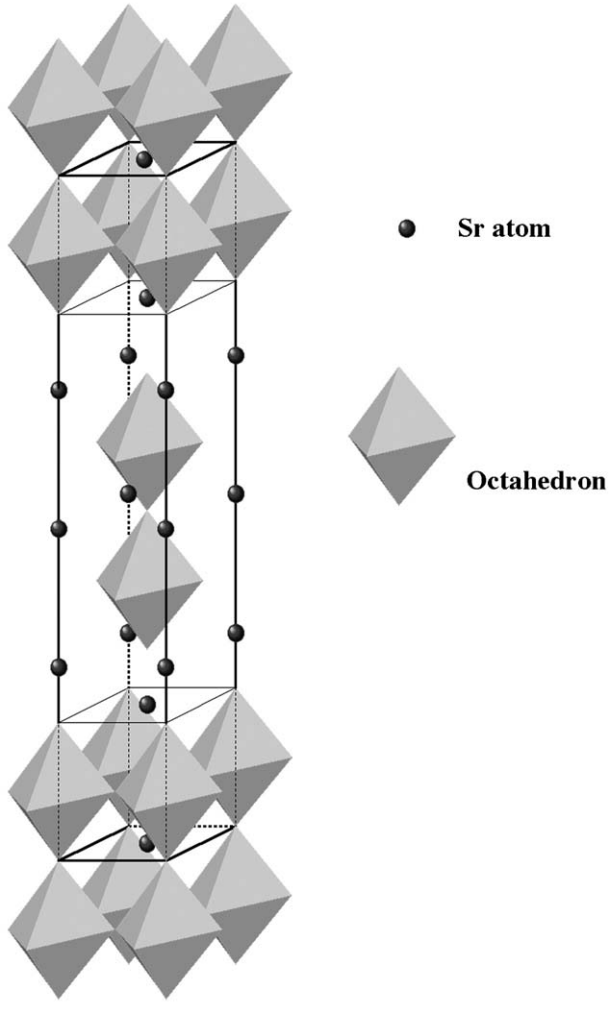

Fig. 1. Crystal lattice of Ruddlesden–Popper structure for $n = 2$. The space group is $I4/mmm$ (No. 139 International Tables). The spheres indicate Sr atoms and the octahedrons indicate IrO_6. An Ir atom is located in the center of the octahedron. Oxygen atoms are located at the corners of the octahedrons.

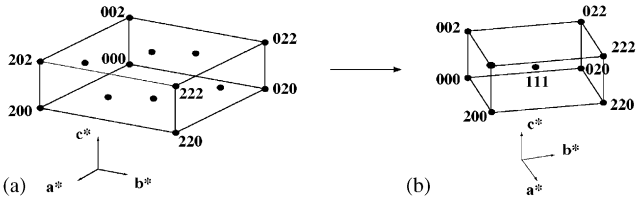

Fig. 2. (a) $I4/mmm$ reciprocal lattice for the crystal structure shown in Fig. 1. (b) A new reciprocal lattice system, which is going to be used in the next section. The 1 1 0 and $1\bar{1}0$ reciprocal points of $I4/mmm$ are chosen to be 2 0 0 and 0 2 0 in this new reciprocal lattice system. The new axes are rotated by 45° with respect to the *c*-axis, and the unit cell length is $\sqrt{2}$ times longer than for $I4/mmm$.

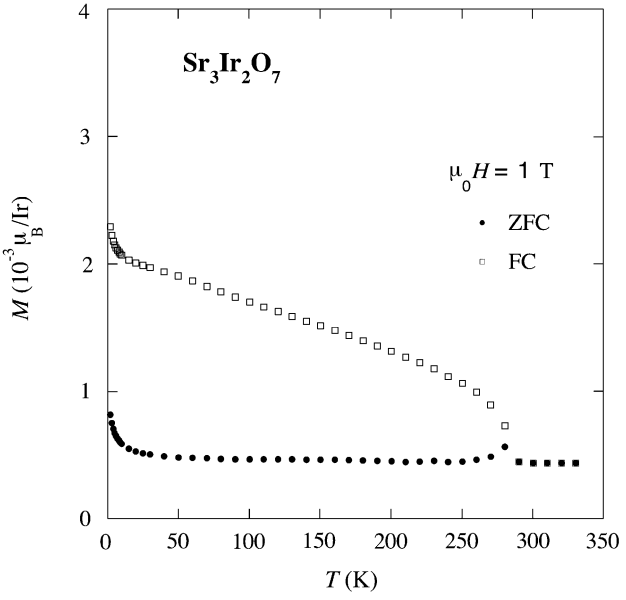

Fig. 3. The temperature dependence of magnetization for $Sr_3Ir_2O_7$ in an FC sequence and a ZFC sequence with $\mu H = 1\,T$.

reciprocal lattice of the Ruddlesden–Popper type structure for $n = 2$. In this figure, the space group is $I4/mmm$ (International Tables No. 139). In the following sections, we use a new coordinate system described in Fig. 2(b) to consider the rotations of IrO_6 octahedrons. New a and b axes were chosen, rotated by 45° with respect to the c-axis.

2. Experiment

Polycrystalline samples of $Sr_3Ir_2O_7$ were synthesized using a high-pressure technique. First, precursors of $Sr_3Ir_2O_7$ were prepared from $SrCO_3$ and IrO_2 with the nominal compositions of $Sr_3Ir_2O_7$. These materials were mixed and heated at 1173 K for 12 h in air. Next, the precursors were placed in gold capsules and pressed up to 2 GPa using a cubic-anvil-type high-pressure apparatus at room temperature. The specimens were then heated up to 1273 K, held at this temperature for 2 h, and finally cooled down to room temperature. The samples were found to be almost single phase, except for tiny amounts of $SrIrO_3$ impurity. Estimated lattice parameters, assuming the tetragonal parent structure, are $a = 3.9026$ Å and $c = 20.9300$ Å, which agrees with the previous report [15]. DC magnetization was measured using a SQUID magnetometer (Quantum Design MPMS). Thin specimens for the TEM were prepared by ion milling. TEM observations were carried out using a JEM 4000FX instrument operated at 100–200 kV to reduce radiation damage. Parallel beam diffraction and convergent beam electron diffraction (CBED) patterns

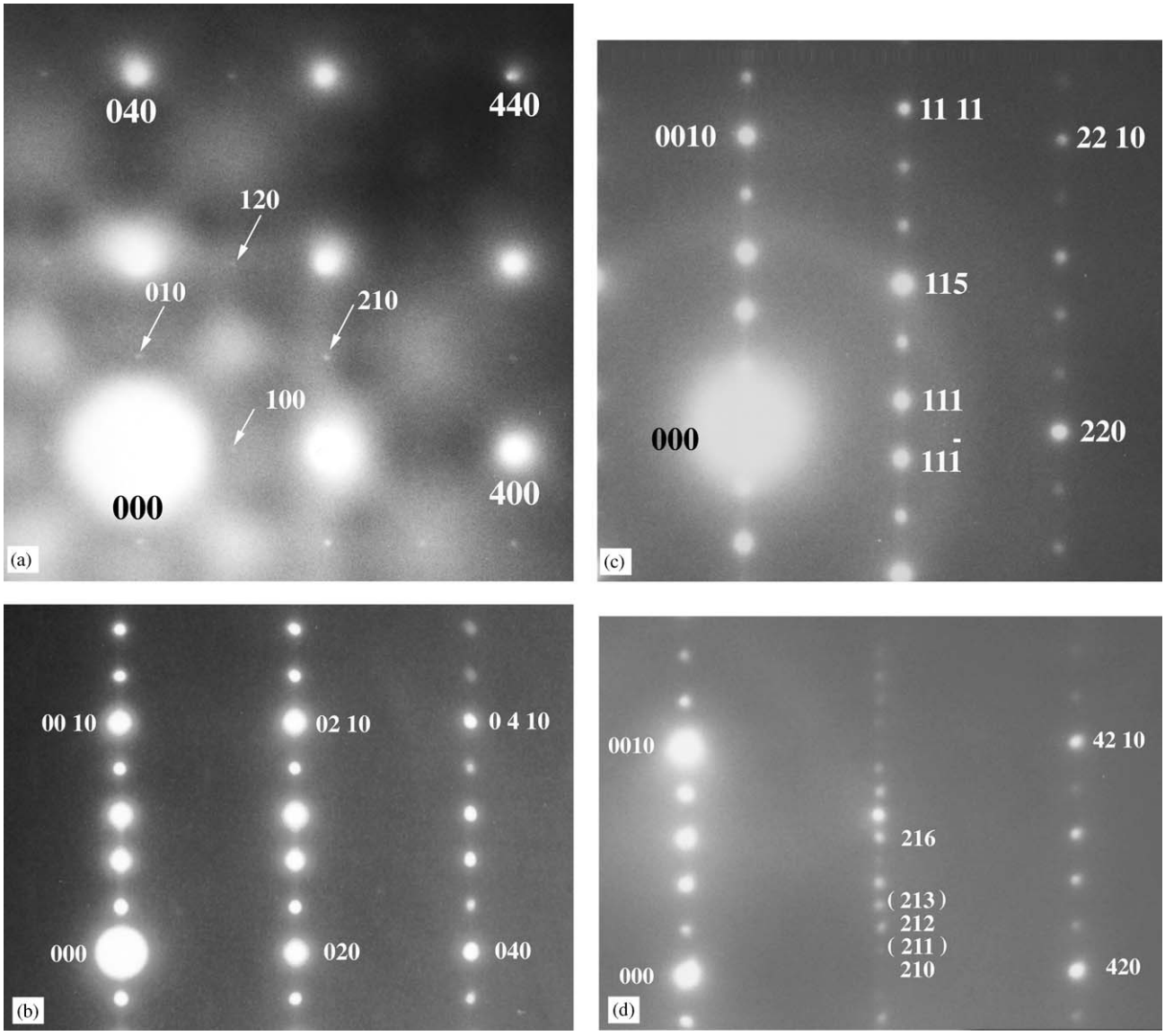

Fig. 4. Parallel beam electron diffraction patterns observed at 315 K, at (a) the [001] zone axis, and at (b) the [100] zone axis direction. White arrows indicate weak intensities observed at the [001] zone axis. Diffraction pattern at (c) $[1\,\bar{1}\,0]$ zone axis and (d) $[1\,\bar{2}\,0]$ zone axis.

were observed at various crystallographic orientations. A Gatan double-tilt N_2 cooling stage was used at 315, 200, and 125 K. Observations at 315 K were performed using an electric heater equipped for the cooling stage. In a typical transmission electron microscope, it is known that the leakage of magnetic field is in the range of 2 T in the specimen chamber from the objective electron lens. We concluded this had no particular influence on the magnetic transition of $Sr_3Ir_2O_7$, because this is similar and the comparable range to the magnetization experiment.

3. Results and discussion of the structure at 315 K

First, the magnetization of the specimens was confirmed. Fig. 3 shows the measured DC magnetization of the specimen in the temperature range from 1.8 to 330 K, in a field cooled sequence (FC), and a zero field cooled sequence (ZFC) at a field of $\mu_0 H = 1$ T. The graph indicates that the magnetic transition occurs at ~280 K. A substantial increase in magnetization is observed below this temperature. The significant difference between the ZFC and FC plots clearly indicates a ferromagnetic component. This result agrees with previously reported results [13–15].

TEM observations indicate that the sizes of the polycrystalline grains were more than several micrometers. Some grains were large enough to be considered as single crystals and were chosen for the investigation. Fig. 4 shows parallel beam electron diffraction patterns observed at the [001], [100] (or [010]), [1 $\bar{1}$ 0], and [1 $\bar{2}$ 0] zone axes orientations, taken at 315 K. Those indices of reflections are given by the new system introduced in Fig. 2(b). In Fig. 4(a) reflections of h, $k = 2n$, such as 2 0 0, 4 0 0, 0 2 0, 0 4 0, 2 2 0, 4 4 0 are observed clearly. Very weak diffracted intensities at $h + k = 2n + 1$, such as 1 0 0, 0 1 0, 2 1 0, …., are observed. However, reflections such as 0 1 0, 0 3 0, 1 0 0, 3 0 0, …., are not observed in Fig. 4(b) at the [100] orientation. We took a number of diffraction patterns of [100] and/or [010] zone axes orientations using different crystals, however reflections of 1 0 0, 3 0 0, …., h 0 0 ($h = 2n + 1$), 0 1 0, 0 3 0, …., 0 k 0 ($k = 2n + 1$), were not observed. We concluded that weak reflections such as 1 0 0, 3 0 0, …. , h 0 0 ($h = 2n + 1$), 0 1 0, 0 3 0, …., 0 k 0 ($k = 2n + 1$), at the [001] zone axis in Fig. 4(a) are due to multiple scattering via higher-order Laue zones. This is a typical phenomenon in a structure belonging to the nonsymmorphic space group; see for example [18]. In the present case, for the [001] zone axis for example, an electron is scattered to an hkl reflection on a higher order Laue zone, and then comes back to the position of the 1 0 0 reflection on the zeroth order Laue zone by a scattering of $-h + 1$, $-k$, $-l$. Both reflections of hkl and $-h + 1$, $-k$, $-l$ are supposed to be allowed reflections, and this scattering process can yield intensity at the 1 0 0 position, where the structure factor itself has a zero value. In the observation at the [001] zone axis, the length of the c* vector is very short, so that the scattering processes involving higher order Laue zones can take place much more strongly than the case at the [100] zone axis observation.

At the [1 $\bar{2}$ 0] zone axis in Fig. 4(d), a series of reflections 2 1 1, 2 1 2, 2 1 3, 2 1 4, …., appears, indicating that the structure is not $I4/mmm$ since reflections do not exist at such positions in $I4/mmm$. Moreover, it looks as if it has a periodicity of double cell along the c-axis

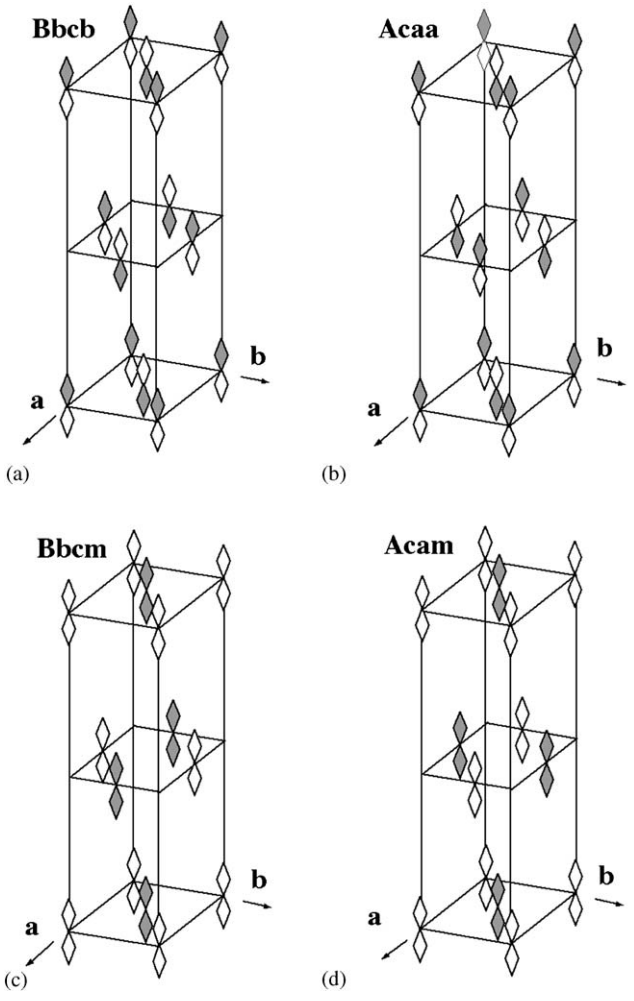

Fig. 5. Model structures for the Ruddlesden–Popper type crystal of $n = 2$ with rotated octahedrons. Dark octahedrons represent counterclockwise rotation with respect to the c-axis, and bright octahedrons represent clockwise rotation. (a) Structure of *Bbcb*, and (b) *Acaa*. In these structures, the rotation directions of vertical neighboring pairs are opposite. In (a), a shift of + (0.5, 0, 0.5) gives an identical structure. In (b) a shift of + (0, 0.5, 0.5) gives an identical structure. Both structures belong to No. 68 in the International Tables for Crystallography. (c) *Bbcm* and (d) *Acam*. In these two structures, the rotation directions of vertical neighboring pairs are the same. In (c), a shift of + (0.5, 0, 0.5) gives an identical structure. In (d) a shift of + (0, 0.5, 0.5) gives an identical structure. Both structures belong to No. 64 in the International Tables for Crystallography.

direction. Also, the very weak reflection 2 1 0 is observed. Therefore, whether the reflection 2 1 0 in Fig. 4(a) and (d) is due to the multiple scattering, or is a genuine reflection seems uncertain. This weak reflection, 2 1 0, observed in Fig. 4(a) and (d) will be discussed later.

The structure of this crystal can now be discussed considering the results observed in Fig. 4. The presence of rotated oxygen octahedrons in this structure has been reported previously [16]. Fig. 5 shows model structures for the Ruddlesden–Popper type of $n = 2$ with rotated octahedrons. Dark octahedrons represent counter-clockwise rotation with respect to the c-axis, and bright octahedrons represent clockwise rotation. Horizontal neighboring octahedrons always rotate in opposite directions since they are connected by one oxygen atom. For a pair of vertical neighbors, there are two types of rotational configurations. In one type, the rotations are in opposite directions, while in the other type, the rotation is in the same direction for a pair of vertical neighbors. The configuration with the same rotational direction will be discussed later. Let us discuss the case of the opposite rotational direction first. Fig. 5(a) and (b) show structures with opposite rotations for vertical neighboring pairs of octahedrons. The space groups can be described as *Bbcb* for (a) and *Acaa* for (b). Both belong to D_{2h}^{22}, and No. 68 in the International Tables for Crystallography. There is a difference in the vertical stacking of the layers for the rotated octahedrons, between Fig. 5(a) and (b). In the structure described in Fig. 5(a), a shift of $+(0.5, 0, 0.5)$ gives an identical structure. In Fig. 5(b) a shift of $+(0, 0.5, 0.5)$ gives an identical structure. If there is only rotation of the octahedrons without anisotropic distortion, the two structures in Fig. 5(a) and (b) are identical to each other after a 90° rotation of the whole unit cell, i.e., they have the relationship of rotated twins. Fig. 6(a) and (b) show reciprocal lattices for the *Bbcb* and *Acaa*, respectively. The closed circles are positions of the reciprocal points with diffracted intensity, and open circles are the positions where the structure factors are zero. However, diffracted intensity may appear by multiple scattering depending on the incident beam direction. If there are *Bbcb* and *Acaa* domains in a crystal, both reciprocal lattices are superimposed. In this case, a series of reflections of 2 1 1, 2 1 2, 2 1 3, 2 1 4, ... in Fig. 4(d) will appear, and the observed diffraction patterns in Fig. 4 can be explained without any contradictions.

In Fig. 5(a) and (b), we assumed opposite rotations for the octahedrons of vertical neighboring pairs. If we consider the same rotational direction for a pair of vertical neighbors, the space group is either *Bbcm* or *Acam*. Both belong to D_{2h}^{18}, and No. 64 in International Tables for Crystallography. The structures are illustrated in Fig. 5(c) and (d). These two structures have a relationship of rotated twins with respect to the c-axis again. There is the possibility of fine twin domain structure. The reciprocal lattice structures are shown in Fig. 6(c) and (d). Again, the superimposition of the two

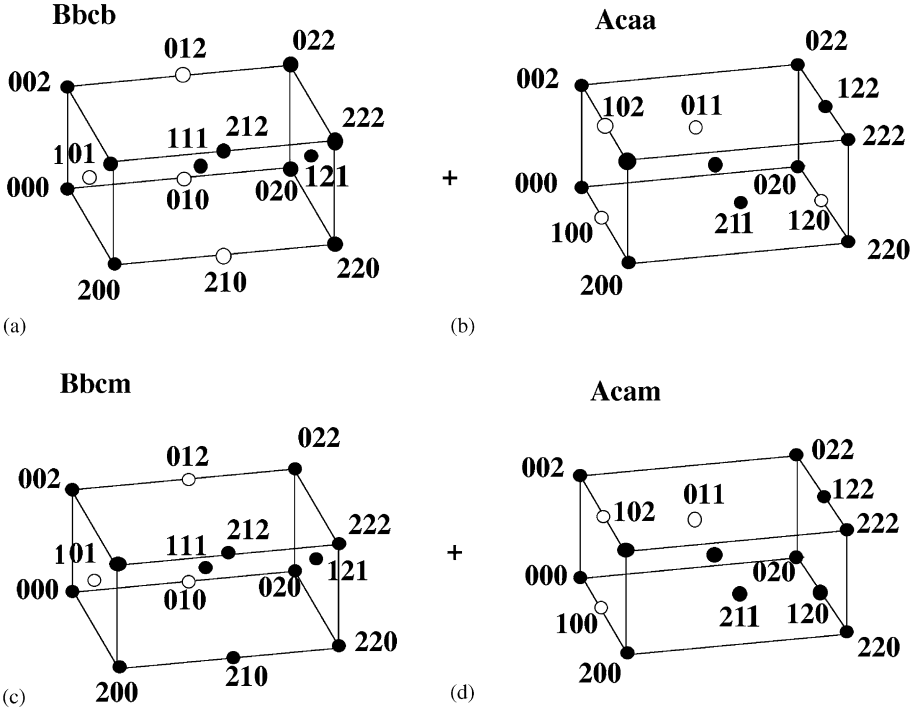

Fig. 6. (a), (b), (c) and (d) represent the reciprocal lattices for the structures shown in Fig. 5, respectively. The closed circles represent the positions of reciprocal points where the diffracted intensities can be observed. The open circles represent the positions where the structure factors have zero-value. However, intensity can appear at these positions depending on incident electron beam orientation due to multiple electron scattering.

reciprocal lattices gives a series of reflections of 2 1 1, 2 1 2, 2 1 3, 2 1 4, …. . However, the structure factors for 2 1 0, 4 1 0…., or 1 2 0, 1 4 0,…. are not zero in these structures. Then, reciprocal points of the 2 1 0 and 1 2 0 reflections become solid circles in Fig. 6(c) and (d), respectively. The issue of the space group, whether it is *Bbcb* (*Acaa*) or *Bbcm* (*Acam*), needs to be considered if the observed weak reflections such as 2 1 0, 4 1 0, …. 1 2 0, 1 4 0, …. are genuine or not. Fig. 7 shows calculated structure factors for electron diffraction as a function of the octahedron rotation angle for the 2 1 0, 2 1 2 reflections in *Bbcb*, 2 1 1, 2 1 3 in *Acaa*, 2 1 0, 2 1 2 in *Bbcm* and 2 1 1 in *Acam*. This figure shows an increase in structure factors as functions of the rotation angle of octahedrons, and indicates that the intensity of the 2 1 0 is stronger than that of the 2 1 2 in *Bbcm* (*Acam*). On the other hand, the 2 1 2 can appear to be stronger than the 2 1 0 in *Bbcb* (*Acaa*). The observed intensity of the 2 1 0 in Fig. 4(d) is much weaker than that of the 2 1 2. Therefore, we conclude that *Bbcm* (and *Acam*) do not fit the experimental results. The weak reflection 2 1 0 observed in Fig. 4(a) and (d) is therefore due to multiple scattering, and the space group is deduced to be *Bbcb* (or *Acaa*) without contradictions.

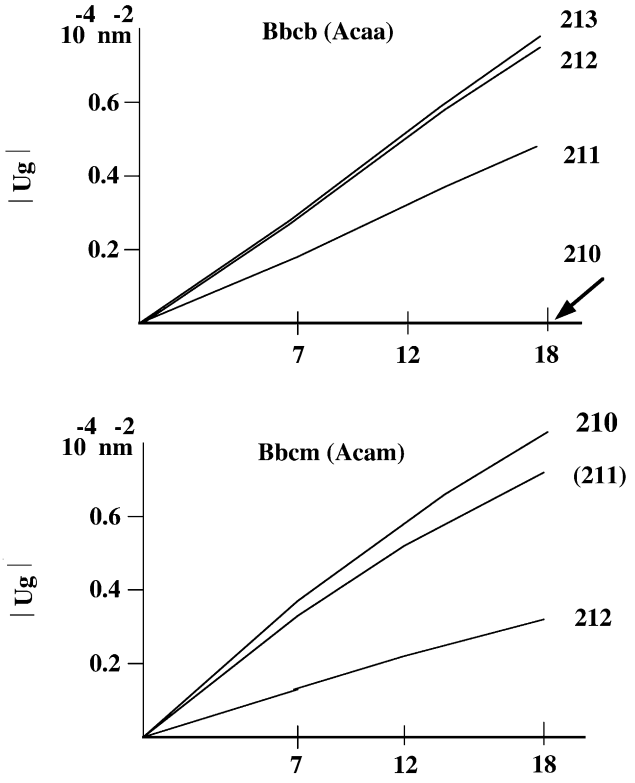

Fig. 7. Calculated structure factors for electron diffraction as a function of the rotation angle of the octahedrons. The vertical axes are absolute values of structure factors (structure potential) U_g. The horizontal axes represent the rotation angle in degrees. The results are shown for reflections of 2 1 0, 2 1 2 of *Bbcb*, and 2 1 1, 2 1 3 of *Acaa* in the upper figure, and reflections of 2 1 0, 2 1 2 of Bbcm, and 2 1 1 of Acam in the lower figure.

The difference in extinction rules between *Bbcb* and *Bbcm* is somewhat critical as seen above. However, differences among other space groups are not that critical. Shaked et al. have analyzed the structure of $Sr_3Ru_2O_7$ by neutron and X-ray diffraction [19,20]. They have discussed the possibility of the structure being $B112/m$ (No. 12), $B112/n$ (No. 15), $Bb2_1m$ (No. 36), *Bbmm* (No. 63), *Bbcm* (No. 64), *Bmcm* (No. 67), *Bbcb* (No. 68), $P4_2/m$ (No. 84), $P4_2/mcm$ (No. 132), and $P4_2/mnm$ (No. 136). They concluded that the structure of $Sr_3Ru_2O_7$ is *Bbcb* (No. 68). Their results for $Sr_3Ru_2O_7$ also agree with the present electron diffraction results for $Sr_3Ir_2O_7$. If we consider not only the rotation but also tilting of the octahedrons, some of the above space groups can be candidates, but we could discard the possibility of the other nine space groups, since they have different extinction rules.

Fig. 8 shows a TEM image taken near the $[1\bar{2}0]$ zone axis orientation. Very fine contrast on the *ab*-plane is observed, these planar defects are concluded to be domain boundaries between the *Bbcb* and *Acaa* lattices, i.e., these structures can be regarded as fine twins with 90° rotation with respect to the *c*-axis. In Fig. 4(b), (c) and (d), weak streaks can be observed along the *c*-axis direction. These streaks may be caused by the presence of fine twins on the *ab*-plane. Subramanian et al. examined the structure of $Sr_3Ir_2O_7$ single crystal by X-ray diffraction [16]. They have discussed the presence of disorder for the rotation of the octahedrons. Their results agree with the fine rotated twin structure observed in this study.

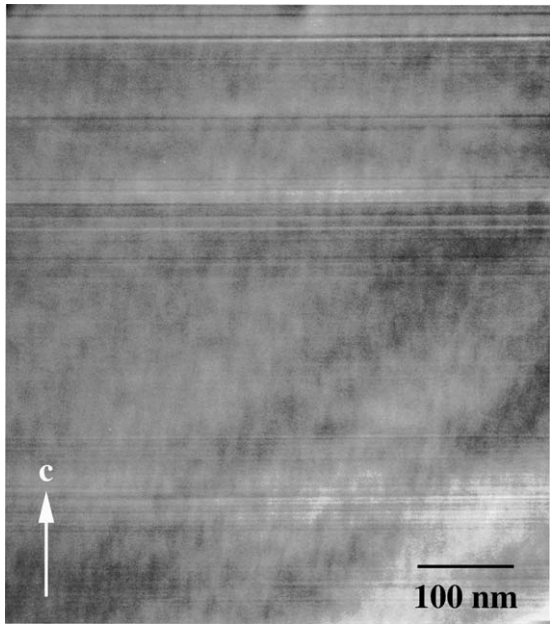

Fig. 8. Bright field TEM image near the $[1\bar{2}0]$ orientation. The very fine twin structure can be observed. Domains of *Bbcb* and *Acaa* have a thin sheet shape and are stacked along the *c*-axis.

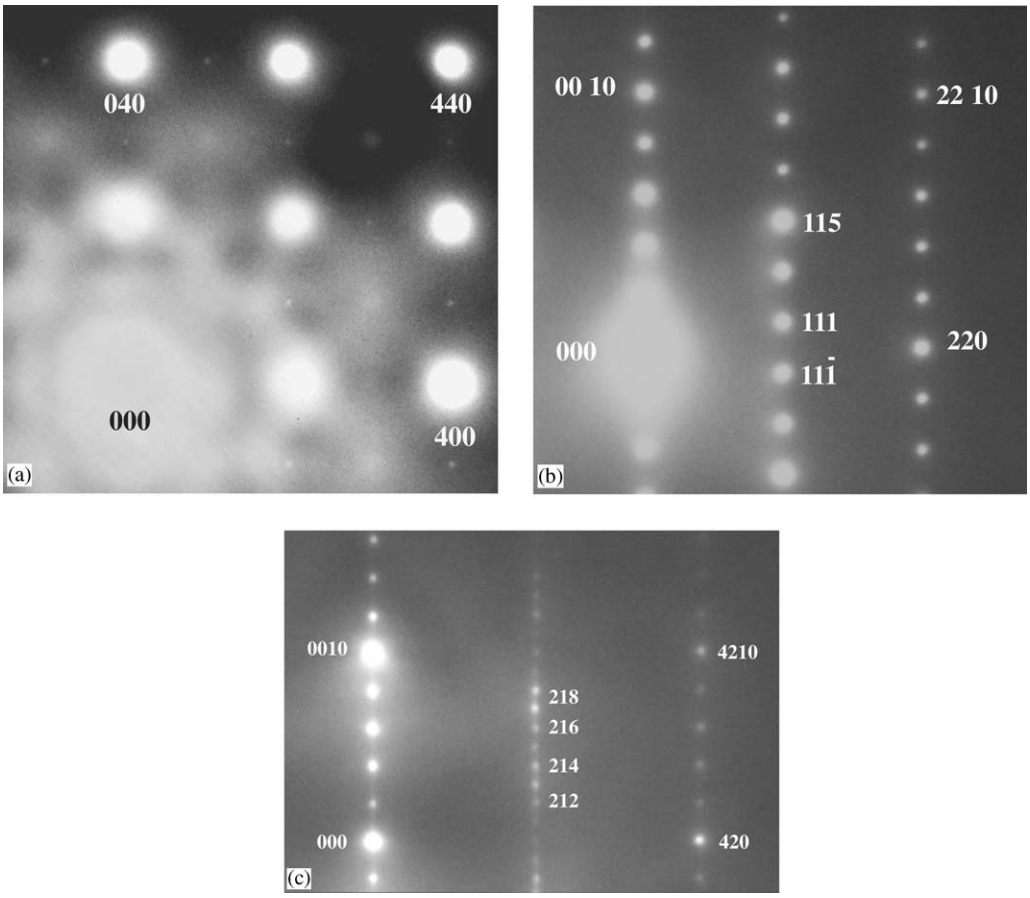

Fig. 9. Diffraction pattern at: (a) [001] zone axis at 200 K, (b) $[1\,\bar{1}\,0]$ zone axis at 200 K, and (c) at $[1\,\bar{2}\,0]$ zone axis at 125 K.

4. Diffraction patterns at low temperatures

When the specimens were cooled to 200 and 125 K, we did not observe appearance of any new reflections. Some examples of the observed electron diffraction patterns are shown in Fig. 9 where (a) is taken at the [001] zone axis at 200 K, (b) is taken at 125 K at $[1\bar{1}0]$, and (c) is taken at the $[1\bar{2}0]$ zone axis orientations. The extinction rules of these observed electron diffraction patterns are identical to those at 315 K. We therefore concluded that there was no change in the space group at lower temperatures. However, the possibility of changes in the rotation angle of the octahedrons still needs to be considered, accompanying the changes in the magnetic properties at ~285 K, similar to the case for $Sr_3Ru_2O_7$ [19]. As shown in Fig. 7, the intensities of superlattice reflections clearly depend on the rotation angle of the octahedrons. We have observed these superlattice reflections several times at 315, 200 and 125 K in fixed positions. However, the intensity changes of these reflections are uncertain. In $Sr_3Ru_2O_7$, the change in the rotational angle has been reported to be more or less than 1° in the region from 0 to 300 K [19]. Such subtle changes in the angle of rotation may be possible.

5. Conclusions

Electron diffraction patterns and transmission electron microscopy images of $Sr_3Ir_2O_7$ were obtained. The space group of this crystal is found to be *Bbcb* (D_{2h}^{22}, No. 68 in the International Tables for Crystallography) at 315 K. The crystal has a fine twin structure with 90° rotation with respect to the *c*-axis. At lower temperatures, at 200 and 125 K, there was no change in the extinction rule in the electron diffraction patterns. Therefore, we concluded there is no change in the space group accompanying the observed change in magnetic properties. However, a possibility of a small change in the rotational angle of IrO_6 octahedrons still remains.

References

[1] Y. Maeno, H. Hashimoto, K. Yoshida, S. Nishizaki, T. Fujita, J.G. Bednoz, F. Lichtenberg, Nature (London) 372 (1994) 532–534.
[2] S. Ikeda, Y. Maeno, M. Nohara, T. Fujita, Physics C 263 (1996) 558–561.
[3] S. Nakatsuji, S. Ikeda, Y. Maeno, J. Phys. Soc. Jpn. 66 (1997) 1868–1871.

[4] S. Ikeda, Y. Maeno, T. Fujita, Phys. Rev. B 57 (1998) 978–986.
[5] S. Ikeda, Y. Maeno, Physica B 259–261 (1999) 947–948.
[6] S. Ikeda, Y. Maeno, S. Nakatsuji, M. Kosaka, Y. Uwatoko, Phys. Rev. B 62 (2000) R6089–R6092.
[7] G. Cao, S. McCall, M. Separd, J.E. Crow, Phys. Rev. B 56 (1997) 321–329.
[8] G. Cao, L. Balicas, Y. Xin, J.E. Crow, C.S. Nelson, Phys. Rev. B 67 (2003) 1,84,405–1,84,412.
[9] G. Cao, L. Balicas, Y. Xin, E. Dagotto, J.E. Crow, C.S. Nelson, Phys. Rev. B 67 (2003) 60,406–66,409.
[10] S. Ikeda, N. Shirakawa, T. Yanagisawa, Y. Yoshida, S. Koikegami, S. Koike, M. Kosaka, Y. Uwatoko, J. Phys. Soc. Jpn. 73 (2004) 1322–1325.
[11] S.A. Grigera, R.S. Perry, A.J. Schofield, M. Chiao, A.J. Millis, A.P. Mackenzie, Science 294 (2001) 329–332.
[12] S. MaCall, G. Cao, J.E. Crow, Phys. Rev. B 67 (2003) 94,427–94,434.
[13] G. Cao, Y. Xin, C.S. Alexander, J.E. Crow, P. Schlottmann, M.K. Crawford, R.L. Harlow, W. Marshall, Phys. Rev. B 66 (2002) 2,14,412–2,14,418.
[14] I. Nagai, S. Ikeda, Y. Yoshida, H. Kito, N. Shirakawa, J. Low Temp. Phys. 131 (2003) 665–669.
[15] I. Nagai, Y. Yoshida, S. Ikeda, H. Matsuhata, H. Kito, M. Kosaka, J. Phys. Soc. Jpn., submitted.
[16] M.A. Subramanian, M.K. Crawford, R.L. Harlow, Materials. Res. Bull. 29 (1994) 645–650.
[17] S.N. Ruddlesden, P. Popper, Acta Cryst. 11 (1958) 54–55.
[18] J. Gjonnes, A.F. Moodie, Acta Cryst. 19 (1965) 65–66.
[19] H. Shaked, J.D. Jorgensen, S. Short, O. Chmaissem, S. Ikeda, Y. Maeno, Phy. Rev. B 62 (2000) 8725–8730.
[20] H. Shaked, J.D. Jorgensen, O. Chmaissem, S. Ikeda, Y. Maeno, J. Solid State Chem. 154 (2000) 361–367.